An egalitarian network model for the emergence of simple and complex cells in visual cortex

L. Tao[1,2], M. Shelley[1], D. McLaughlin[1] and R. Shapley[1]

[1] Courant Institute of Mathematical Sciences
NYU, 251 Mercer Street, New York, NY 10012, and
Center for Neural Science, NYU

4 Washington Place, New York, NY 10003

[2] Department of Mathematical Sciences and
Center for Applied Mathematics and Statistics

New Jersey Institute of Technology, Newark, NJ 07102

CAMS Report 0304-27, Spring 2004

Center for Applied Mathematics and Statistics

NJIT

An Egalitarian Network Model for the Emergence of Simple and Complex Cells in Visual Cortex

Louis Tao,[1,2,3] Michael Shelley,[1,2] David McLaughlin,[1,2] and Robert Shapley[2,1]

[1] *Courant Institute of Mathematical Sciences, New York University, 251 Mercer Street, New York, New York 10027, USA*

[2] *Center for Neural Science, New York University, 4 Washington Place, New York, New York 10003, USA*

[3] *Department of Mathematical Sciences, New Jersey Institute of Technology, 323 Martin Luther King, Jr., Blvd, Newark, New Jersey 07102, USA*

Manuscript information: 17 text pages (including references and figure captions), 6 figures, 116 words in abstract, and less than 33767 characters in paper

Classification: Physical Sciences: Applied Mathematics; Biological Sciences: Neuroscience

Corresponding Author: Michael Shelley, Courant Institute of Mathematical Sciences, New York University, 251 Mercer Street, New York, NY 10027, e-mail: shelley@cims.nyu.edu, Phone (212) 998-3284, Fax (212) 995-4121

Abstract

We explain how Simple and Complex cells arise in a large-scale neuronal network model of the primary visual cortex of the macaque. Our model consists of over 16,000 integrate-and-fire, conductance-based point neurons, representing the cells in a small, 1 mm^2 patch of an input layer of the primary visual cortex. In the model the local connections are isotropic and nonspecific, and convergent input from the lateral geniculate nucleus confers cortical cells with orientation and spatial phase preference. The balance between lateral connections and LGN drive determines whether individual neurons in this recurrent circuit are Simple or Complex. The model reproduces qualitatively the experimentally observed distributions of both extracellular and intracellular measures of Simple and Complex response.

Introduction

A fundamental classification of neurons in the primary visual cortex (V1) is as Simple or Complex[1]. A Simple cell responds to visual stimulation in an approximately linear fashion. For example, when responding to the temporal modulation of standing grating patterns, Simple cells modulate their firing at the stimulus frequency and are sensitive to its spatial phase (or location). Complex cells are very nonlinear, modulating their firing at twice the stimulus frequency and showing little sensitivity to spatial phase.

Simple and Complex cells may have different tasks in visual perception. Cortical cells must represent spatial properties such as surface brightness and color, and the perceptual spatial organization of a scene that is the basis of form. Simple cells are necessary for all of these functions because they are the visual cortical neurons that are able to respond monotonically to signed edge contrast. Complex cells, being insensitive to spatial phase, cannot provide a cortical representation of signed contrast, but they are sensitive to texture, firing at elevated rates in response to stimuli within their receptive fields.

While long-standing and with functional implications, the Simple/Complex classification is hardly sharp. Recent work by Ringach *et al* [2] analyzes the extracellular responses of neurons across many experiments in macaque V1. They find that many V1 cells are neither wholly Simple nor wholly Complex, but lie somewhere in between. And while most cells in V1 might be classified as Complex, the cortical layer which receives the bulk of LGN excitation, $4C$, has Simple and Complex cells in approximately equal proportion.

These data about the properties and proportions of Simple and Complex cells must reflect the nature of synaptic connectivity of the cortex, but as yet no theoretical model provides a unified accounting of how they might arise. Associated with the Simple/Complex classification is the influential hierarchical model of Hubel & Wiesel[1], wherein Simple cells receive geniculate drive, and their pooled output drives the Complex cells. As we argue in *Results*, this conception seems difficult to reconcile with the experimental evidence. Here we study a large-scale model of the neuronal dynamics in layer $4C\alpha$ of macaque V1, whose architecture is better known than for almost any other cortical area. Our model is egalitarian, with local lateral connectivity being *nonspecific* and *isotropic*. In Wielaard *et al* [3] we showed how strong network inhibition within such an architecture could ameliorate the nonlinearities of LGN excitation, and so give rise to a network of Simple cells. That work showed that cortico-cortical excitatory conductances

resembled the spiking responses of Complex cells.

Our new model cortex naturally produces Simple cells, Complex cells, and cells with intermediate responses. While strong cortico-cortical inhibition remains an important feature, a new and central assumption of this model is that the strength of LGN excitation varies broadly, so that some cortical cells receive significant LGN drive, while others receive little. This is combined with the constraint that the total synaptic drive onto each cell is approximately constant, though divided between geniculate and striate sources, as is suggested by theories of cortical development[4, 5] and by recent experiments[6]. Through a balance of strong recurrent excitation and inhibition this model yields Complex responses in those cells with relatively little LGN drive. Simple cells arise in a manner similar to those of the Wielaard *et al* model. Recurrent excitation is also the feature used by Chance, Nelson, & Abbott in their conceptual model of Complex cells [7]. In our conductance-based, point-neuron model, we find that recurrent excitation can be destabilizing, and that its control requires slow synaptic excitation.

We show that this egalitarian model, which combines natural assumptions on the variability of cortical and geniculate drive and what is known about the neuronal architecture of V1, can rationalize many aspects of the available experimental data. The model yields physiologically reasonable Simple and Complex cell responses, both in the rate and the form of spiking. The architecture leads to distinctive predictions of population measures of Simple/Complex responses, which have the qualitative structure seen in recent experimental measurements. Our work here may prove important for understanding the roles of network excitation and inhibition in other cortical areas.

Results

Figure 2a,b shows experimental data of De Valois *et al* [8], based on extracellular recordings of spikes, that illustrate the differing spatial summation properties of Simple and Complex cells in macaque V1 (see also[9, 10]). Fig. 2a shows a Simple cell's response to contrast reversal stimulation by a standing sine-wave pattern (here, "contrast reversal" is the sinusoidal modulation in time of the contrast of the pattern). Response to contrast reversal is a critical test of linearity in Simple cells[8, 11]. The cell's response depends strongly upon the spatial phase or position of the standing grating pattern

relative to the midpoint of the neuron's receptive field, has a large amplitude response at the fundamental driving frequency at one spatial phase (the "preferred-phase"), and very little response at the "orthogonal phase", 90° away. Response at both of these phases shows little or no generation of the higher temporal harmonics that might be expected for a nonlinear system. On the other hand, nonlinear harmonic distortion products are apparent in the responses of cortical Complex cells[8], as shown in Fig. 2b. In particular, its temporal response shows little sensitivity to spatial phase, and firing modulates at twice the stimulus frequency (i.e., at the 2^{nd} harmonic). While these cells in De Valois *et al* [8] were not assigned to a cell layer, subsequent experimental work in recording the activity of neurons across all layers of macaque V1 has found many neurons in layer $4C\alpha$ that behave just as these two cells do[2].

Simple and Complex cell responses, like those seen in experiment, arise in our model cortex. For contrast reversal stimulation, Fig. 2c shows a model cell responding like a Simple cell, and Fig. 2d shows another cell responding like a Complex cell. These are but two cells taken from a large-scale network simulation with $\sim 16,000$ cells (75% excitatory, 25% inhibitory). The architecture of this network is presented schematically in Fig. 1. Some of the crucial distinguishing features of the model, derived from biological data, are that the local lateral connectivity is *nonspecific* and *isotropic*, with lateral monosynaptic inhibition acting at shorter length-scales than excitation[12, 13, 14, 15]. Orientation and spatial phase preferences are conferred on cortical cells from the convergence of output from many LGN cells[16], with orientation preference laid out in pinwheel patterns[17, 18, 19, 20], and spatial phase preference varying widely from cortical cell to cortical cell[21].

As Fig. 1 also indicates, the number of LGN cells, N_{LGN}, whose afferents impinge on a model cortical cell varies broadly and randomly from cortical cell to cortical cell. Much of the evidence for variability in the strength of LGN drive is indirect[22, 23, 24], and so for the purposes of this study, we make the simplest assumption and take the distribution of N_{LGN} to be uniform. A model Simple cell like the cell depicted in Fig. 2c has a nearly maximal number of LGN afferents (conceptually, Neuron 1 in the schematic), while a Complex cell (like the one in Fig. 2d) has few LGN afferents (conceptually Neuron 3 in the schematic). Figure 3 shows the model Simple cell's instantaneous and cycle-averaged intracellular conductances and effective reversal potential V_S (both normalized as described in *Methods*) at the (a) preferred and (b) orthogonal phases of contrast reversal, over one cycle

of stimulation. (In our network, the membrane time-scale is very short[25], and hence the intracellular potential closely tracks V_S when below the firing threshold, here normalized to unity. When V_S is above unity, the cell is typically firing.) At the preferred phase, the excitatory conductance from the LGN is a rectified sinusoidal wave peaking at three-quarters cycle, while at orthogonal phase the LGN excitation is frequency doubled. Both the rectification at preferred, and the frequency doubling at orthogonal phase, follow from the rectification nonlinearities of individual LGN cells[3]. Not shown is the response to the stimulus phase 180° away from preferred, for which the LGN excitation is nearly identical but peaking instead at one-quarter cycle. Intermediate phases of stimulation appear as combinations of these half-wave rectified and frequency doubled wave-forms (see Fig. 2 of Wielaard *et al* [3]).

As the spatial phase preference conferred by the LGN drive varies widely from cortical cell to cortical cell, a stimulus phase that is preferred for one cortical cell will for other cells be at preferred, orthogonal, or intermediate phases. For cells with fewer LGN afferents than our model Simple cell, all of these basic wave-forms of LGN excitation persist, but are diminished in magnitude. An extreme example of this is the sample Complex cell, whose intracellular responses are shown in Fig. 3c at the first phase presented in Fig. 2d. This cell has no LGN afferents, and hence no LGN excitation.

Thus, because of the diverse nature of its LGN input, particularly in input phases, the model cortex receives an LGN excitation that for some cells is peaked in the first half-period of stimulation, peaked in the second half for others, and for yet others is peaked in both halves (i.e., stimulus is at F_2). Consequently the bulk visual excitation – LGN excitation averaged over all cells – peaks in both halves of the period of stimulation, and is insensitive to phase. In a network that is isotropically and nonspecifically coupled, a cell samples through its cortico-cortical conductances the activity of many other cells, each excited by the LGN at a different input phase. A natural consequence is that these conductances reflect the bulk forcing and so are frequency doubled and phase insensitive. This is illustrated in Fig. 3: Both the inhibitory and excitatory cortico-cortical conductances of the Simple cell are frequency doubled and practically identical at the two phases shown, as indeed they are also for the other intermediate phases. These observations hold true for the cortico-cortical conductances of the Complex cell; Examination at all of its phases of response would show near invariance to phase, and frequency doubling.

Phase insensitivity and frequency doubling are key to how this network

produces both Simple and Complex cells. For example, Fig. 3B shows that LGN excitation is frequency doubled at the orthogonal phase, yet this strong nonlinearity in the LGN input is not expressed in the spiking of the cell. As explained in Wielaard *et al* [3], if excitation and cortico-cortical inhibition are roughly in balance, phase insensitive cortico-cortical inhibition is sufficient to suppress frequency-doubled firing at the orthogonal phase.

Another structural element of the model network is indicated in Fig. 1: The number of excitatory, LGN afferents driving a cortical cell is inversely correlated to the number of excitatory cortico-cortical afferents. That is, the fewer synapses on a cell taken up by the LGN, the more are available to excitatory (presynaptic) neurons in the network. This assumption is based on theories of cortical development in which the number of excitatory synapses is kept constant[4, 5] (recent experiments support this theoretical constraint[6]). The consequences of this assumption are made clear in Fig. 3C. For the Complex cell, the lack of LGN excitation is compensated for by a strong, frequency-doubled cortico-cortical excitation, balanced by likewise frequency-doubled inhibition. The firing pattern of the cell is then naturally frequency-doubled, and phase insensitive, as is observed for Complex cells.

Figure 1 also illustrates that we use slow excitation in the synapses between cortical cells (see temporal coupling profiles). The total EPSP was the sum of an AMPA component and an NMDA component[26] with equal weight integrated over time. We found that, in networks where the cortical coupling is mediated only by AMPA, the strong cortical amplification led to large-amplitude global oscillations. The slow excitation provided by NMDA was necessary to achieve stability in the recurrent network[27]. Another feature of this model that differentiates it from Wielaard *et al* [3] is the presence of a global inhibition and excitation that is modulated by total network activity. This global coupling could be interpreted, for example, as being mediated through layer 6 feedback to layer 4C, and does not affect Simple/Complex population responses. Its main effect is to improve orientation selectivity within the layer, and to remove some of the differences in network activity near and far from the pinwheel centers of orientation hypercolumns[28].

Another common visual stimulus used to classify the response properties of cortical neurons is drifting sinusoidal gratings (a traveling, spatially modulated intensity pattern, held at a fixed orientation). While often used to probe selectivities for orientation, frequency, or direction, this stimulus also shows characteristic differences between Simple and Complex cells. For the model Simple and Complex cells of Figs. 2 and 3, Fig. 4 shows their extra-

and intracellular responses to a drifting grating stimulus (8 Hz at optimal orientation and spatial frequency). Their extracellular spiking is typical of experimentally observed Simple and Complex cells: The Simple cell follows the temporal modulation of the drifting grating as it moves across its receptive field, while the Complex cell shows an elevated, mostly unmodulated firing over the whole cycle of stimulation.

Examination of LGN and cortico-cortical conductances in Fig. 4 accounts for the model's response to drifting gratings. First, the strong LGN excitation into the Simple cell modulates with the stimulus frequency. Different cells receive LGN excitation of similar wave-form, but due to variability in both the number of LGN afferents, and in spatial phase preference, they are diverse in both amplitude and time of peak excitation. For drifting grating stimulation, this yields a bulk forcing to the model cortex that is nearly uniform in time and which manifests itself as nearly time-invariant cortico-cortical conductances[3]. Thus, for the model Simple cell, both the intracellular V_S and its extracellular firing pattern modulate on the time dependence of its LGN input. Conversely, for the model Complex cell both V_S and the firing pattern are driven by the unmodulated cortico-cortical conductances, and hence show only elevated, unmodulated responses.

Given the structure of the model cortex, it is clear that our two sample cells, one Simple and one Complex, must sit within a continuum of possible intracellular and extracellular responses. We explore this with a standard characterization of response: Figure 5a shows the histogram of *modulation ratio* F_1/F_0 for the cycle-averaged effective reversal potential, V_S, across the whole population of $\sim 12,000$ excitatory cells within the model cortex. The modulation ratio is the ratio of first harmonic amplitude (at the stimulus frequency) to the mean. Cells with flat intracellular responses, like the sample Complex cell in Fig. 4b, have small modulation ratios. The distribution of modulation ratio is broad, unimodal and monotonically decreasing, and reflects the broad distribution in number of LGN afferents and the constraint of fixed, total excitation. There are actually recent experimental data with which to compare. Fig. 5b shows the modulation ratio of the intracellular potential for 168 cells in cat cortex, measured recently by David Ferster and colleagues (personal communication). It shows surprisingly good qualitative agreement with our theoretical model by also showing a broad and unimodal distribution. (The long tail of the experimental data comprises only 10% of the cells.)

Curiously, this unimodality is not preserved in extracellular measures,

neither in experiment nor in the model. Fig. 5a shows for the model cortex the distribution of modulation ratio of the cycle-averaged firing rate, while Fig. 5b shows the measured distributions from Ringach *et al* [2] for 308 cells in macaque V1, and for the 38 located in $4C$. Following others (e.g. [29, 2]), we use this extracellular F_1/F_0 as a classifier, labeling as Simple those cells with $F_1/F_0 > 1$ (red in the figure), and as Complex those with $F_1/F_0 < 1$ (blue in the figure). Qualitatively similar, both distributions show a bimodal structure peaked near the extremes of the classifier, but with a large proportion of cells having responses neither wholly Simple, nor wholly Complex.

On the basis of a simple model, Mechler & Ringach[30] have recently showed that spike-rate rectification could lead to a bimodal distribution in extracellular F_1/F_0, even though intracellular response is unimodally distributed. Our work here shows that this result can arise within a cortical model which incorporates many elements that are biologically realistic. We note that a robust result of our model is the unimodal intracellular distribution of F_1/F_0. However, to achieve a bimodal extracellular distribution requires that recurrent excitation be sufficiently strong and so create a sizable population of Complex cells.

Figure 6 shows how membrane conductances relate to extracellular F_1/F_0. First, as expected, the more "Simple" a cell, the stronger its LGN excitation, but it is also true that even very Simple cells can receive substantial network excitation. Second, it is clear that LGN and cortico-cortical excitation are generally anti-correlated, with very Complex cells receiving almost exclusively cortical excitation. Cortico-cortical inhibition, being roughly uniform in time, can adjust the DC component of the extracellular spiking and vary the modulation ratio. Here, cortico-cortical inhibition is large and is much more uniform than excitation with respect to F_1/F_0. Finally, across the whole population note that the total conductance is large, having increased over background values by factors of two or three, and is dominated by inhibition (as in Wielaard *et al* [3]). Such large inhibitory conductance increases have been found in recent intracellular measurements[31, 32, 33], and their effect on cortical function has been studied theoretically[25].

Discussion

The main results of this paper are these: We have constructed a cortical model, based on Macaque V1, for the emergence of Simple and Complex cells within the same basic circuit. Their differing responses reflect differing proportions of geniculate versus cortico-cortical excitation. While the amount of excitation is kept roughly fixed, its division varies widely from cell to cell, as do many other elements of the model, such as strength of coupling and of extra-cortical drive, and the receptive field properties of LGN excitation. In a manner consistent with experiment measurement, many cells emerge as Complex, many as Simple, and many as being mixed. We predict a bimodal but broad structure of extracellular modulation ratio, itself arising from a distribution of intra-cellular modulation ratios that is broad *but* monotonic. This prediction is consistent with available data.

Our model is very different from the influential hierarchical model of Hubel & Wiesel[1], wherein Simple cells receive geniculate drive, and their pooled output drives the Complex cells. Clearly, a strict rendering of the Hubel & Wiesel model would yield a bimodal population response in both the extra- and intra-cellular modulation ratio, as is not observed here, nor in experiment. Our model is more egalitarian than hierarchical, with all cell types receiving strong inputs from the network of both simple and complex cells (see Fig. 6) and with almost all cells receiving LGN drive.

In one recent revision of the hierarchical model, Chance, Nelson, & Abbott[7] produced a network of Complex cells through strong cortico-cortical excitation. This is the same feature that produces complex cells in our model. However, theirs is a largely conceptual model, where the network activity is modeled through rate equations, and the cortico-cortical coupling is one-dimensional. Ours models the activity of individual neurons being driven by changes in membrane conductance, and incorporates many other elements of biological realism in the coupling architecture. A more fundamental difference is structural. In Chance *et al* [7], the outputs of simple cells are assumed, and used to drive the complex cell network. As we show in Wielaard *et al* [3], asking how Simple cells can exist within a network setting is a fundamental question, given the nonlinearities of LGN excitation, and here we show how both Simple and Complex cells can arise within the same network. In our model, as in the model of Wielaard *et al* , it is strong network inhibition that produces the nearly linear responses of Simple cells. However, the present model is distinctly different from the Simple cell network in Wielaard *et al*

[3]. The presence of strong recurrent cortico-cortical excitation in the present model creates the Complex cells, and in this way makes the present model's behavior resemble that of V1.

Methods

Our model cortex consists of approximately $16,000$ coupled excitatory and inhibitory integrate-and-fire (I&F) point neurons, whose intracellular potentials follow:

$$\begin{aligned} \frac{dv^j}{dt} &= -g_L(v^j - V_L) - g_E^j(t)(v^j - V_E) - g_I^j(t)(v^j - V_I) \qquad (1) \\ &= -g_T^j(t)(v^j - V_S^j(t)), \end{aligned}$$

where g_L is the leak conductance; $g_E^j(t)$ and $g_I^j(t)$ are the excitatory and inhibitory conductances, respectively. Here, the conductances have been normalized by the membrane capacitance, leaving them with dimensions of inverse time (e.g. $g_L = 50\ sec^{-1}$). V_L, V_E, and V_I are the rest, excitatory and inhibitory reversal potentials, respectively. In I&F dynamics, when the membrane potential hits a threshold, V_T, a spike is recorded and v^j is instantaneously reset to V_L. An action potential is associated with a spike-time and conductance changes are then distributed throughout the network. Potentials are non-dimensional with $V_T = 1$, $V_L = 0$, and by using the commonly accepted values for the various biophysical parameters [34], $V_E = 4.67$, $V_I = -0.67$. In Eq. (1), $g_T = g_L + g_E^j + g_I^j$ is the total membrane conductance and $V_S^j = (V_E g_E^j + V_I g_I^j)/g_T^j$ is the effective (time-dependent) reversal potential. We use a modified fourth-order Runge-Kutta method [35] with 0.1 ms time-steps.

To close the model, we need to specify g_E^j and g_I^j; In short, these conductances are produced by firing activity within the model cortex, from spikes arriving from the LGN, and from spiking of extra-cortical sources. A major part of the connectivity is described through Fig.1 and its explication in *Results*, and many further details are given in **Supplementary Information** (on-line).

Acknowledgments

We thank Dario Ringach, John Rinzel and Haim Sompolinsky for their critical comments. This work was supported by NSF grants DMS-9971813 and DMS-0211655, NEI grant R01 EY-01472 and the Sloan-Swartz Program in Theoretical Neurobiology at NYU.

References

[1] Hubel, D & Wiesel, T. (1962) *J Physiol (Lond)* **160**, 106–154.

[2] Ringach, D, Shapley, R, & Hawken, M. (2002) *J. Neuroscience* **22**, 5639–5651.

[3] Wielaard, J, Shelley, M, Shapley, R, & McLaughlin, D. (2001) *J. Neuroscience* **21**, 5203–5211.

[4] Miller, K & MacKay, D. (1994) *Neural Computation* **6**, 100–126.

[5] Miller, K. (1996) *Neuron* **17**, 371–374.

[6] Royer, S & Pare, D. (2002) *Neuroscience* **115**, 455–462.

[7] Chance, F, Nelson, S, & Abbott, L. (1999) *Nature Neuroscience* **2**, 277–282.

[8] De Valois, R, Albrecht, D, & Thorell, L. (1982) *Vision Res* **22**, 545–559.

[9] Movshon, J, Thompson, I, & Tolhurst, D. (1978) *J Physiol (Lond)* **283**, 79–99.

[10] Reid, R, Soodak, R, & Shapley, R. (1991) *J. Neurophysiol.* **66**, 505–529.

[11] Spitzer, H & Hochstein, S. (1985) *J.Neurophysiol* **53**, 1244–1265.

[12] Fitzpatrick, D, Lund, J, & Blasdel, G. (1985) *Journal of Neuroscience* **5**, 3329–3349.

[13] Lund, J. (1987) *Journal of Comparative Neurology* **257**, 60–92.

[14] Callaway, E & Wiser, A. (1996) *Visual Neuroscience* **13**, 907–922.

[15] Callaway, E. (1998) *Ann. Rev. Neurosci.* **21**, 47–74.

[16] Reid, R & Alonso, J.-M. (1995) *Nature* **378**, 281–284.

[17] Bonhoeffer, T & Grinvald, A. (1991) *Nature* **353**, 429–431.

[18] Blasdel, G. (1992) *Journal of Neuroscience* **12**, 3115–3138.

[19] Blasdel, G. (1992) *Journal of Neuroscience* **12**, 3139–3161.

[20] Maldonado, P, Godecke, I, Gray, C, & Bonhoeffer, T. (1997) *Science* **276**, 1551–1555.

[21] DeAngelis, G, Ghose, R, Ohzawa, I, & Freeman, R. (1999) *Journal of Neuroscience* **19**, 4046–4064.

[22] Tanaka, K. (1985) *Vis. Res.* **25**, 357–364.

[23] Alonso, J.-M, Usrey, W. M, & Reid, R. (2001) *J. Neurosci.* **21**, 4002–4015.

[24] Ringach, D. (2002) *J. Neurophysiol.* **88**, 455–463.

[25] Shelley, M, McLaughlin, D, Shapley, R, & Wielaard, J. (2002) *J. Comp. Neurosci.* **13**, 93–109.

[26] Rivadulla, C, Sharma, J, & Sur, M. (2001) *J. Neurosci.* **21**, 1710–1719.

[27] Wang, X. (1999) *J. Neuroscience* **19**, 9587–9603.

[28] McLaughlin, D, Shapley, R, Shelley, M, & Wielaard, J. (2000) *Proc. Natl. Acad. Sci. USA* **97**, 8087–8092.

[29] Skottun, B, DeValois, R, Grosof, D, Movshon, J, Albrecht, D, & Bonds, A. (1991) *Vis. Res.* **31**, 1079–1086.

[30] Mechler, F & Ringach, D. (2002) *Vis. Res.* **42**, 1017–1033.

[31] Borg-Graham, L, Monier, C, & Fregnac, Y. (1998) *Nature* **393**, 369–373.

[32] Hirsch, J, J.M.Alonso, Reid, R, & Martinez, L. (1998) *J. Neuroscience* **15**, 9517–9528.

[33] Anderson, J, Carandini, M, & Ferster, D. (2000) *J. Neurophysiol.* **84**, 909–926.

[34] Koch, C. (1999) *Biophysics of Computation.* (Oxford University Press, Oxford).

[35] Shelley, M & Tao, L. (2001) *J. Comput. Neurosci.* **11**, 111–119.

Figure Captions

Figure 1: Schematic of Model. Upper panel: Inputs from visual stimulation is relayed through the LGN. Each V1 cell "sees" a collection of LGN cells that is probabilistically sampled from a two-dimensional Gabor function. The segregation of convergent On- and Off-center LGN cells (represented by red and green circles) confers orientation and spatial phase preference on individual cortical cells — these preferences are inherited from parameters of individual Gabor functions. Orientation preference is laid out in pinwheels (map shown in color), while spatial phase preference is distributed randomly (map not shown, but individual phase preferences is shown for 3 sample neurons). The number of LGN cells (N_i) providing afferents varies from cell to cell (shown for sample neurons) and is distributed randomly in cortex (uniformly between 0 and 30). The firing rate of individual LGN cells are modelled as inhomogeneous Poisson processes with rates that are taken from a thresholded, linear spatio-temporal filter (as detailed previously in [28, 3]). Lower left Panel: Intracortical coupling are isotropic with interaction profiles taken to be Gaussians in space (excitation in red and inhibition in blue), with the lengthscale of excitation ($200\,\mu$m) greater than that of inhibition ($100\,\mu$m). Inhibitory coupling strengths are taken randomly from a Gaussian distribution, while excitatory coupling strengths are drawn from Gaussian distributions whose mean strengths are inversely proportional to N_i. The extra $4C\alpha$ conductances have strengths that are also drawn randomly from Gaussian distributions. Lower right panel: Each EPSP is taken to be 50% AMPA and 50% NMDA, while an IPSP is divided evenly between GABA_A and a slower inhibition (based on recent experimental findings of B. Connors).

Figure 2: Simple and Complex cell responses to contrast reversal stimulation (8 spatial phases, at optimal orientation, and temporal and spatial frequency). **A** and **B** are from experiments of DeValois *et al* [8] (with permission), while **C** and **D** are neurons from the model network. **A**: Macaque Simple cell driven at 2 Hz. The spatial phase is defined so that one spatial cycle of the grating pattern is 360°. At 180°, the response is zero. **B**: Macaque Complex cell driven at 2 Hz. The response is at the second harmonic and is insensitive to spatial phase. **C**: Model Network Simple cell driven at 4 Hz. **D**: Model Network Complex cell driven at 4 Hz.

Figure 3: Extra- and intracellular responses to 4 Hz contrast reversal. **A** and **B** show the model Simple Cell in **Fig. 2C** responding at its preferred and orthogonal spatial phases. **C** shows the model Complex Cell in **Fig. 2D** at one of the phases. From left to right: cycle-averaged firing rate (with the spontaneous rate in red dashes); effective reversal potential V_S (magenta); LGN-driven conductance (green); cortico-cortical excitatory conductance (red); cortico-cortical inhibitory conductance (blue). Dotted lines are standard deviations for each of the conductances and for the potential. Thin black lines indicate instantaneous values of conductances and potentials. Cycle averages are performed over 24 cycles.

Figure: 4: Responses to 8 Hz drifting grating at optimal orientation. **A** shows the model Simple cell in **Fig. 2C**. **B** shows the model Complex cell in **Fig. 2D**. From left to right: cycle-averaged firing rates (spontaneous rates as dashed red lines); effective reversal potential V_S (magenta); LGN-driven conductance (green); cortico-cortical excitatory conductance (red); cortico-cortical inhibitory conductance (blue). The dotted lines are standard deviations for each of the conductances and for the potential. The thin black lines indicate instantaneous values of conductances and potentials. Cycle-averages are performed over 48 cycles.

Figure 5: Comparison of intracellular and extracellular F_1/F_0 between model and experiment. **A**: Distribution of F_1/F_0 of membrane potential (relative to background activity) of excitatory neurons in model network, when stimulated at optimal orientation and spatial frequency. The height of each bar indicates the total number of excitatory neurons in each bin, while the blue and red portions correspond to the cells that are classified as "Simple" or "Complex" based on their extracellular responses. **B**: Distribution of F_1/F_0 of membrane potential in experiment of Ferster et al. in cat primary visual cortex (unpublished data, replotted by F. Mechler, and reprinted here with permission). **C**: Distribution of the modulation ratio F_1/F_0 of excitatory neurons in model network. (The distribution for the inhibitory population is qualitatively similar.) **D**: Distribution of the modulation ratio F_1/F_0 of 308 cells from the experiments of Ringach *et al* [2] (with permission). The detail shows the distribution for the 38 cells identified as being in $4C$. Here, with a baseline of zero firing rate, the modulation ratio is bounded between zero and two.

Figure 6: Time-averaged conductances as a function of the (extracellular) modulation index F_1/F_0: green is LGN-driven conductance; red is cortico-cortical excitation; blue is cortico-cortical inhibition and black is total conductance. Each point is computed by finding the population of neurons within a certain range in F_1/F_0, and then averaging (over the population and over time). The vertical bars at each point denote population average of the standard deviation.

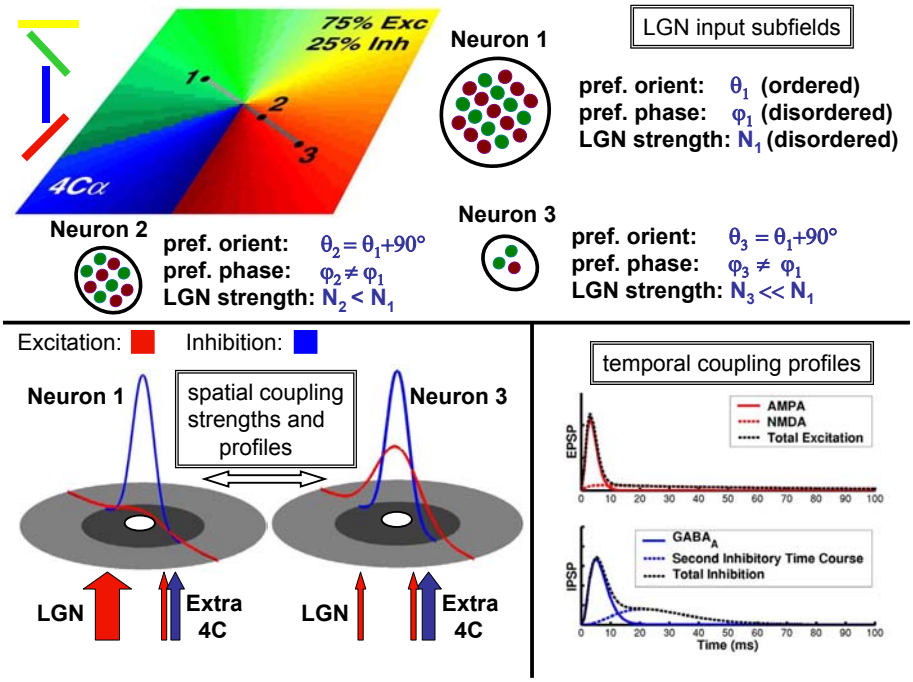

Figure 1: Schematic of Model. Upper panel: Inputs from visual stimulation is relayed through the LGN. Each V1 cell "sees" a collection of LGN cells that is probabilistically sampled from a two-dimensional Gabor function. The segregation of convergent On- and Off-center LGN cells (represented by red and green circles) confers orientation and spatial phase preference on individual cortical cells — these preferences are inherited from parameters of individual Gabor functions. Orientation preference is laid out in pinwheels (map shown in color), while spatial phase preference is distributed randomly (map not shown, but individual phase preferences is shown for 3 sample neurons). The number of LGN cells (N_i) providing afferents varies from cell to cell (shown for sample neurons) and is distributed randomly in cortex (uniformly between 0 and 30). The firing rate of individual LGN cells are modelled as inhomogeneous Poisson processes with rates that are taken from a thresholded, linear spatio-temporal filter (as detailed previously in [28, 3]). Lower left Panel: Intracortical coupling are isotropic with interaction profiles taken to be Gaussians in space (excitation in red and inhibition in blue), with the lengthscale of excitation (200 μm) greater than that of inhibition (100 μm). Inhibitory coupling strengths are taken randomly from a Gaussian distribution, while excitatory coupling strengths are drawn from Gaussian distributions whose mean strengths are inversely proportional to N_i. The extra $4C\alpha$ conductances have strengths that are also drawn randomly from Gaussian distributions. Lower right panel: Each EPSP is taken to be 50% AMPA and 50% NMDA, while an IPSP is divided evenly between $GABA_A$ and a slower inhibition (based on recent experimental findings of B. Connors).

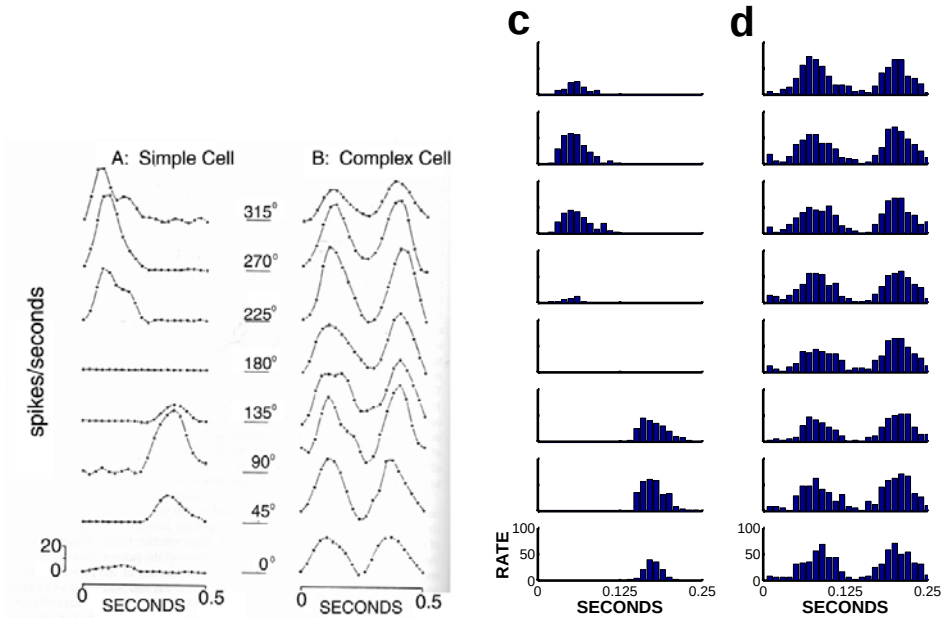

Figure 2: Simple and Complex cell responses to contrast reversal stimulation (8 spatial phases, at optimal orientation, and temporal and spatial frequency). **A** and **B** are from experiments of DeValois *et al* [8] (with permission), while **C** and **D** are neurons from the model network. **A**: Macaque Simple cell driven at 2 Hz. The spatial phase is defined so that one spatial cycle of the grating pattern is 360°. At 180°, the response is zero. **B**: Macaque Complex cell driven at 2 Hz. The response is at the second harmonic and is insensitive to spatial phase. **C**: Model Network Simple cell driven at 4 Hz. **D**: Model Network Complex cell driven at 4 Hz.

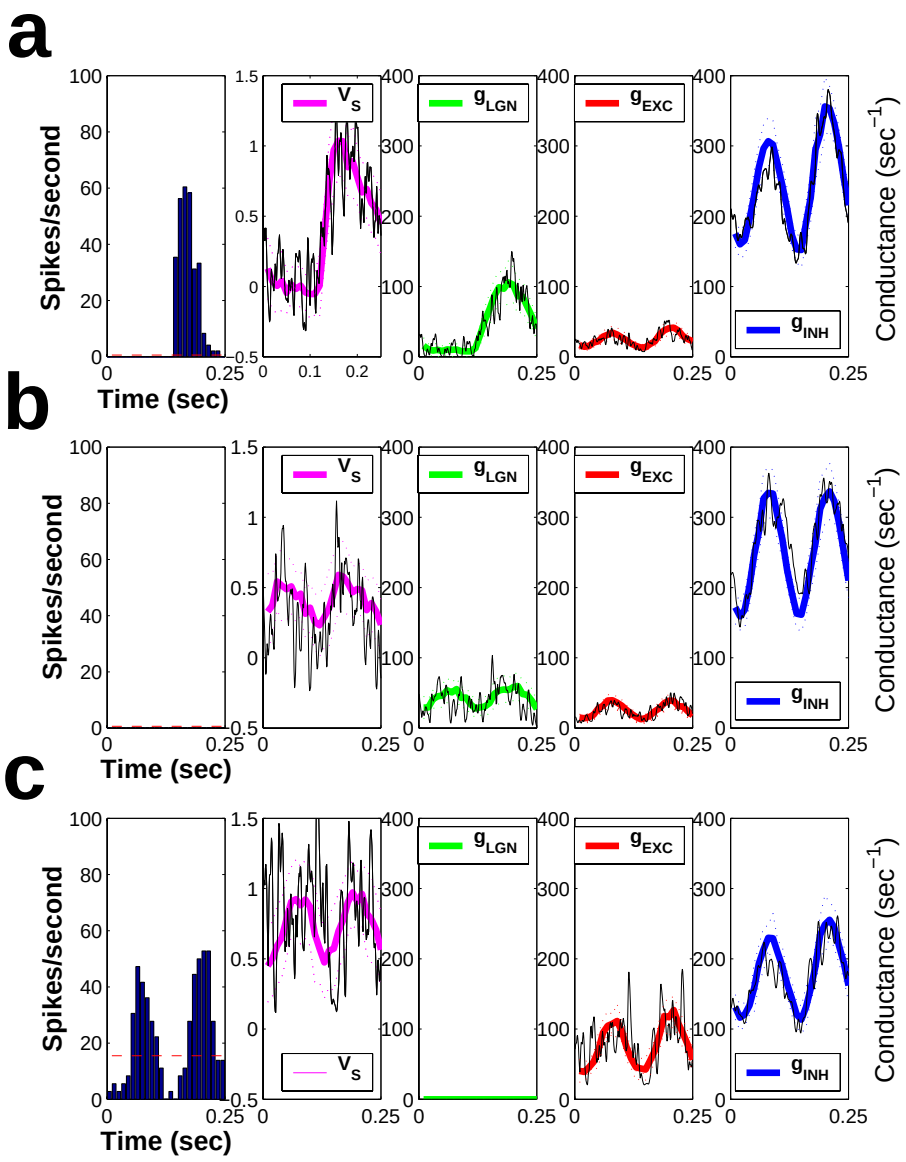

Figure 3: Extra- and intracellular responses to 4 Hz contrast reversal. **A** and **B** show the model Simple Cell in **Fig. 2C** responding at its preferred and orthogonal spatial phases. **C** shows the model Complex Cell in **Fig. 2D** at one of the phases. From left to right: cycle-averaged firing rate (with the spontaneous rate in red dashes); effective reversal potential V_S (magenta); LGN-driven conductance (green); cortico-cortical excitatory conductance (red); cortico-cortical inhibitory conductance (blue). Dotted lines are standard deviations for each of the conductances and for the potential. Thin black lines indicate instantaneous values of conductances and potentials. Cycle averages are performed over 24 cycles.

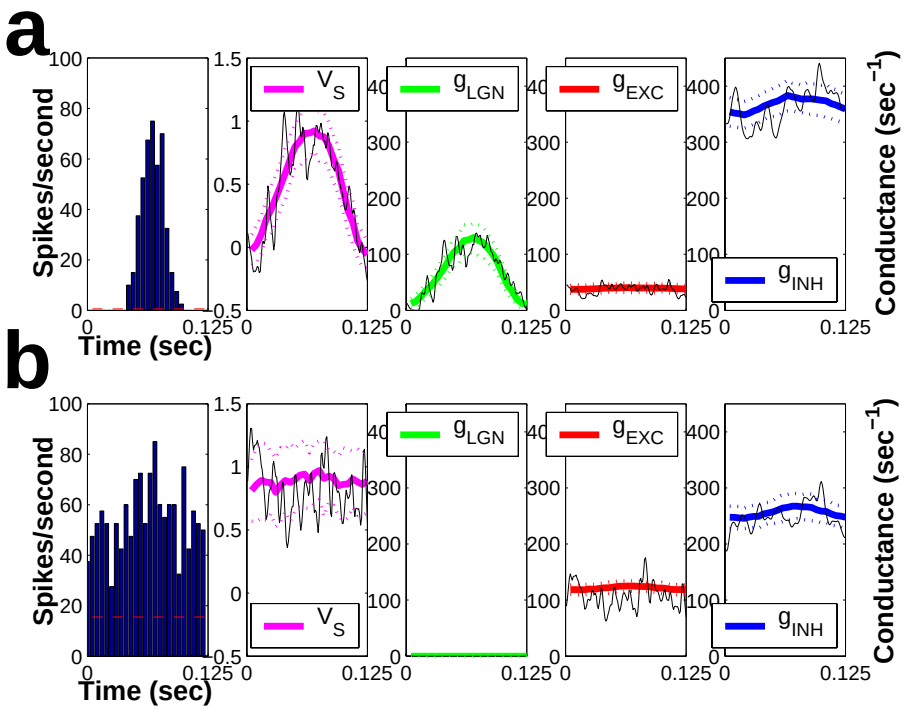

Figure 4: Responses to 8 Hz drifting grating at optimal orientation. **A** shows the model Simple cell in **Fig. 2C**. **B** shows the model Complex cell in **Fig. 2D**. From left to right: cycle-averaged firing rates (spontaneous rates as dashed red lines); effective reversal potential V_S (magenta); LGN-driven conductance (green); cortico-cortical excitatory conductance (red); cortico-cortical inhibitory conductance (blue). The dotted lines are standard deviations for each of the conductances and for the potential. The thin black lines indicate instantaneous values of conductances and potentials. Cycle-averages are performed over 48 cycles.

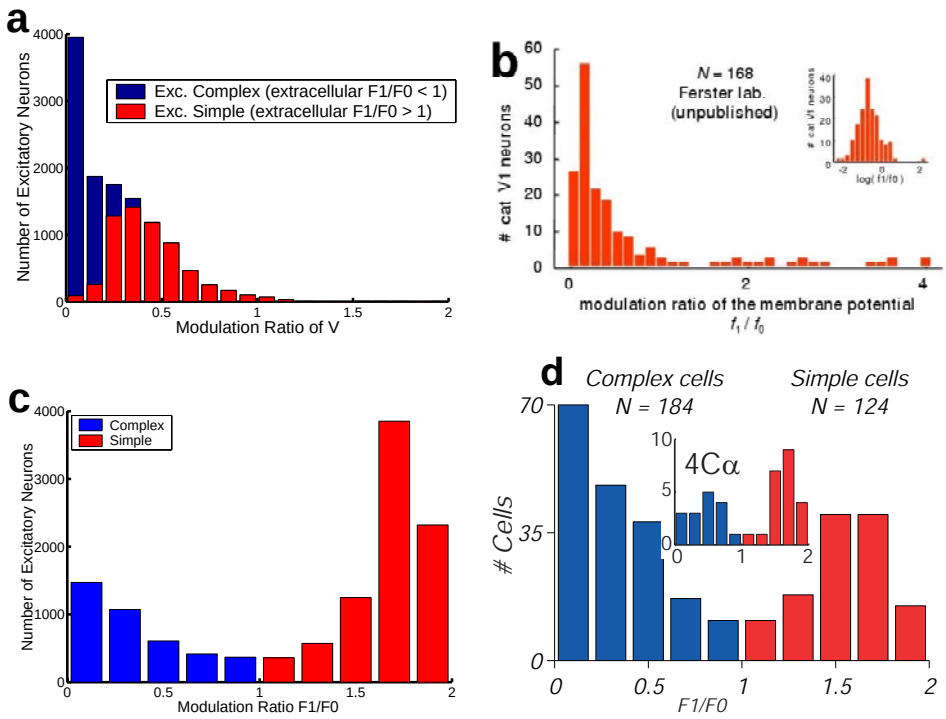

Figure 5: Comparison of intracellular and extracellular F_1/F_0 between model and experiment. **A**: Distribution of F_1/F_0 of membrane potential (relative to background activity) of excitatory neurons in model network, when stimulated at optimal orientation and spatial frequency. The height of each bar indicates the total number of excitatory neurons in each bin, while the blue and red portions correspond to the cells that are classified as "Simple" or "Complex" based on their extracellular responses. **B**: Distribution of F_1/F_0 of membrane potential in experiment of Ferster et al. in cat primary visual cortex (unpublished data, replotted by F. Mechler, and reprinted here with permission). **C**: Distribution of the modulation ratio F_1/F_0 of excitatory neurons in model network. (The distribution for the inhibitory population is qualitatively similar.) **D**: Distribution of the modulation ratio F_1/F_0 of 308 cells from the experiments of Ringach *et al* [2] (with permission). The detail shows the distribution for the 38 cells identified as being in $4C$. Here, with a baseline of zero firing rate, the modulation ratio is bounded between zero and two.

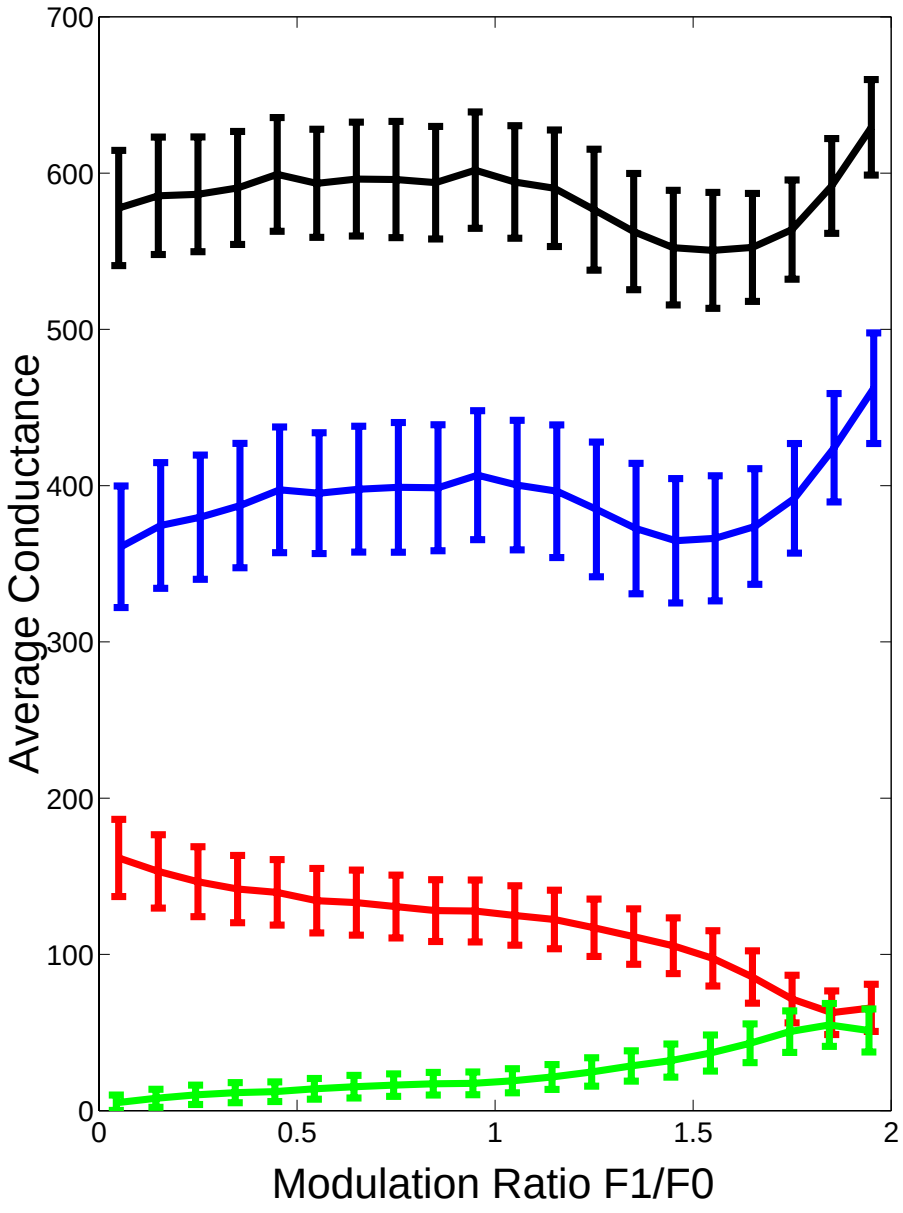

Figure 6: Time-averaged conductances as a function of the (extracellular) modulation index F_1/F_0: green is LGN-driven conductance; red is cortico-cortical excitation; blue is cortico-cortical inhibition and black is total conductance. Each point is computed by finding the population of neurons within a certain range in F_1/F_0, and then averaging (over the population and over time). The vertical bars at each point denote population average of the standard deviation.